doi:10.1006/jmbi.2001.5279 available online at http://www.idealibrary.com on IDEAL® J. Mol. Biol. (2002) 315, 831–843

JMB

The ATPase Domain of SecA Can Form a Tetramer in Solution

Brian R. Dempsey[1], Anastassios Economou[2], Stanley D. Dunn[1] and Brian H. Shilton[1]*

[1]*Department of Biochemistry University of Western Ontario London, ON N6A 5C1, Canada*

[2]*Institute of Molecular Biology and Biotechnology and Department of Biology University of Crete, P.O. Box 1527, GR-71110 Iraklio, Crete Greece*

**Corresponding author*

Preprotein translocase is a general and essential system for bacterial protein export, the minimal components of which are SecA and SecYEG. SecA is a peripheral ATPase that associates with nucleotide, preprotein, and the membrane integral SecYEG to form a translocation-competent complex. SecA can be separated into two domains: an N-terminal 68 kDa ATPase domain (N68) that binds preprotein and catalyzes ATP hydrolysis, and a 34 kDa C-terminal domain that regulates the ATPase activity of N68 and mediates dimerization. We have carried out gel filtration chromatography, analytical ultracentrifugation, and small-angle X-ray scattering (SAXS) to demonstrate that isolated N68 self-associates to form a tetramer in solution, indicating that removal of the C-terminal domain facilitates the formation of a higher-order SecA structure. The associative process is best modelled as a monomer-tetramer equilibrium, with a K_D value of 63 μM^3 (where $K_D = [\text{monomer}]^4/[\text{tetramer}]$) so that at moderate concentrations (10 μM and above), the tetramer is the major species in solution. Hydrodynamic properties of the N68 monomer indicate that it is almost globular in shape, but the N68 tetramer has a more ellipsoidal structure. Analysis of SAXS data indicates that the N68 tetramer is a flattened, bi-lobed structure with dimensions of approximately 13.5 nm × 9.0 nm × 6.5 nm, that appears to contain a central pore.

© 2002 Academic Press

Keywords: preprotein translocase; SecA; ATPase domain; oligomerization; small-angle X-ray scattering

Introduction

Preprotein translocase is an essential and general secretory system found in prokaryotic organisms (for recent reviews, see Driesen *et al.*,[1] Economou[2] and Müller *et al.*[3]). The minimal components of preprotein translocase are SecYEG and SecA.[4–6] SecYEG is membrane-embedded, contains sequence homology to functionally related molecules in the endoplasmic reticulum[7,8] and may form a protein conducting channel.[9,10] SecA is a peripheral ATPase that associates with SecYEG, binds the substrate preprotein, and catalyzes ATP hydrolysis with coupled movement of the preprotein through SecYEG and into the periplasm.[11,12]

The mechanism of protein translocation has been the subject of intense study for a number of years. During translocation, SecA binds ATP and preprotein and interacts with membrane-embedded SecYEG such that both a 65 kDa domain and a 30 kDa domain are stabilized against proteolysis.[13,14] Each cycle of ATP binding and hydrolysis results in translocation of approximately 5 kDa of preprotein,[15,16] and therefore repeated cycles of ATP hydrolysis would be required to translocate the entire preprotein. In this model, ATP binding[17] is thought to initiate profound conformational changes in SecA, such that most of the SecA molecule becomes resistant to proteolysis[14,18] and accessible from the periplasmic side of the translocon.[19–21]

Data on the structure and composition of the SecA-SecYEG complex need to be integrated with this model of translocation. Detergent-solubilized SecYEG undergoes a monomer-tetramer equilibrium in solution and two-dimensional crystals of SecYEG do not contain a ring-like structure,

Abbreviations used: SAXS, small angle X-ray scattering; R_g, radius of gyration; STEM, scanning transmission electron microscope; AMP-PNP, adenylylimidodiphosphate; rms, root-mean-square.

E-mail address of the corresponding author: bshilton@uwo.ca

0022-2836/02/040831–13 $35.00/0

© 2002 Academic Press

suggesting that the protein-conducting channel is assembled from multiple SecYEG complexes.[22] Recent scanning transmission electron microscopy (STEM) studies indicate that detergent-solubilized SecYEG exists as monomers and dimers, and that these are assembled by SecA-(AMP-PNP) to form a tetrameric complex (i.e. Sec$(YEG)_4$).[23] Furthermore, arrested translocation reactions were found to contain particles of mass 531 and 686 kDa, which are thought to comprise preprotein substrate, SecA dimer, and either two or four SecYEG heterotrimers. On the other hand, there is biochemical evidence that the active translocon contains only a monomeric SecYEG complex.[24] SecA is a dimer in solution[25,26] and it was proposed to function as a dimer when bound to SecYEG at the membrane.[27] SecA undergoes conformational changes upon nucleotide binding, as assessed by intrinsic fluorescence, differential scanning calorimetry,[28] and protease sensitivity,[29] but SAXS indicates that changes in the structure of SecA in solution are relatively modest.[26]

Knowledge of the subunit stoichiometry and structure of this SecA-SecYEG complex is a crucial prerequisite to understanding the mechanism of translocation. One approach that is being used to understand the translocation mechanism is to dissect the system into smaller domains and investigate the function and interactions between these domains. The SecA protomer can be divided into two domains: an N-terminal domain, from residues 1-610, and a C-terminal domain, from 610 to 901.[30] The N-terminal ATPase domain contains seven consensus DEAD helicase motifs,[31,32] including the Walker A and B motifs[33] that are critical for high affinity nucleotide binding and hydrolysis,[34] and it also contains a preprotein cross-linking site.[35] The N-terminal domain is able to bind peptides corresponding to signal sequences, and this binding decreases the intrinsic ATPase activity of the domain.[36] Finally, the N-terminal domain appears to be largely responsible for SecYEG binding.[37] The C-terminal domain is important for mediating dimer formation between SecA protomers;[38,39] it has an important role in regulating the ATPase activity and ligand-binding properties of the N-terminal domain,[32,36,39] and is also required for binding to SecB.[40]

We are interested in the mechanisms by which SecA couples ATP binding and hydrolysis to interactions with preprotein and SecYEG. In solution, the C-terminal domain of SecA has been shown to suppress the ATPase activity of the N-terminal domain.[39] Based on this observation, the high ATPase activity of SecA during active translocation[11] may be due, at least in part, to an altered position of the C-terminal relative to the N-terminal domain when SecA is bound to SecYEG. Here we show that, in solution, absence of the C-terminal domain has a profound effect on the structure of the N-terminal domain; that is, the isolated N-terminal domain is able to form an oligomeric complex, which we demonstrate is a tetramer. This result was unexpected in light of previous work, in which the N-terminal domain was shown to be monomeric when assessed by chemical cross-linking and/or gel filtration chromatography.[38,39] The ability of the N-terminal domain of SecA to form a tetramer is interesting in view of the oligomeric state of the translocase subunits with which SecA interacts. Specifically, SecA interacts with SecB, which is a dynamic tetramer, or more precisely, a dimer of dimers.[41,42] There is evidence that SecYEG also forms tetramers during active translocation.[23] SecA protomer-protomer interactions may be important in the assembly and regulation of the active translocation complex. To develop these ideas further, we have carried out a detailed study of the oligomerization and overall shape of the isolated N-terminal ATPase domain from *Escherichia coli* SecA.

Results

Expression, purification, and characterization of N68

N68 comprises the N-terminal 610 residues of SecA.[39] We expressed *E. coli* N68 as an isolated polypeptide containing a hexa-histidine tag at the N terminus to facilitate purification; incorporation of this hexa-histidine tag yields a fully functional full-length His_6-SecA molecule.[32] Purified N68 had the expected ATPase activity (not shown) and was exceptionally stable: after seven days of sedimentation equilibrium experiments (20 °C, no nucleotides) the purified protein yielded a single band when analyzed by SDS-PAGE (Figure 1(a)). There is a single cysteine residue in N68, and we noticed a tendency for N68 to form disulfide-bonded dimers. We included reducing agents for all analyses to ensure that large molecular mass species were formed *via* non-covalent interactions; nevertheless, small amounts of disulfide-bonded dimers did form over time. After seven days of sedimentation equilibrium experiments, N68 was run under non-reducing conditions, and a faint band migrating with a M_R of 138 kDa was seen (Figure 1(a)). Analysis by densitometry indicated that this band represented no more than 8 % of the total protein.

Gel filtration analysis of N68

Purified His_6-N68 was analyzed by gel filtration chromatography. At 10 mg/ml (Figure 1(c)) N68 elutes with an apparent M_R of 250 kDa, somewhat larger than full-length SecA (Table 1) and there is a distinct shoulder on the main peak of N68 (Figure 1(c)), indicating the presence of smaller species. The lack of a large peak at the void position in the chromatogram (7.5 ml; Figure 1(c)) indicates that the protein preparation does not form extremely large, non-specific aggregates. Rather, the apparent M_R of N68 decreased as the protein was diluted (Table 1); for example, at

0.2 mg/ml, N68 migrated with an M_R of 115 kDa (Figure 1(d)).

Associative properties of N68: sedimentation equilibrium

The presence of a higher M_R species in gel filtration experiments indicated that N68 was forming an oligomeric species, either a very elongated dimer or a more globular trimer or tetramer. We used sedimentation equilibrium, the results of which are completely independent of a molecule's shape, to measure the molecular mass and associative properties of N68. To verify that the higher molecular mass species represents reversibly self-associating N68, a plot of apparent molecular mass as a function of protein concentration was used (Figure 2(a)). The concentration gradients were produced at 10,000 rpm using three different protein concentrations, and it can be seen that the three plots coincide, indicative of a self-associating system. If the larger molecular mass species were due to polydispersity in the protein preparation, one would expect that the same molecular mass distribution would be produced at each protein concentration and the plots would not coincide.[43]

To determine the optimal model and an accurate association constant, a comprehensive analysis of N68 self-association was carried out using four rotor speeds, 7000, 8500, 10,000, and 13,000 rpm, and three protein concentrations, 0.7, 0.35, and 0.14 mg/ml, at 20 °C. Fitting these data as a single species yielded molecular masses of approximately 170 kDa and obvious systematic errors (not shown). However, the experimental data were very well modelled using a monomer-tetramer equilibrium with the association constant (K_A) and concentration of monomer at the reference radius (C_0) as the sole variables. In this case, when the protein concentration of 0.35 mg/ml was used with the four rotor speeds (a total of 12 curves), the value for the K_A was 0.016 μM^{-3}, which corresponds to a K_D value of 63 μM^3 (where $K_D = [\text{monomer}]^4/[\text{tetramer}]$). An example of the fit obtained with this model is given in Figure 2(b). Other possible models for the self association of N68 were tested. Inclusion of a dimer in the monomer-tetramer model did not significantly improve the agreement with experimental data, and there were clear systematic errors for a dimer-tetramer equilibrium (not shown). Sedimentation equilibrium analysis carried out at 4 °C yielded a K_D value of 84 μM^3, indicating that the formation of the tetramer was not strongly temperature depen-

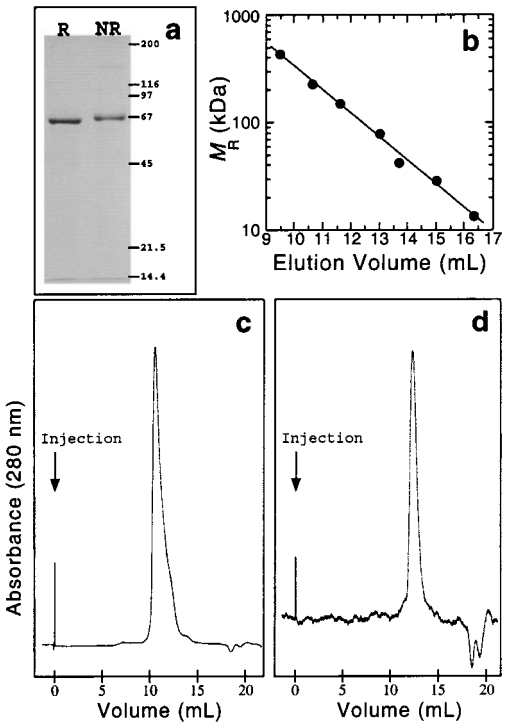

Figure 1. SDS-PAGE analysis and gel filtration chromatography of N68. (a) Purified N68 was used for sedimentation equilibrium studies and at the end of the experiments (seven days at 20 °C) was analyzed by SDS-PAGE under reducing (R) or non-reducing (NR) conditions. (b) Calibration curve for gel filtration column. Molecular mass standard proteins were chromatographed on an HR 10/30 column of Superdex 200 at a flow rate of 0.5 ml/minute. The running buffer was 50 mM Tris-HCl, 100 mM KCl, 5 mM $MgCl_2$, 1 mM EDTA, and 5 mM β-mercaptoethanol (pH 8.0). Absorbance at 280 nm was monitored and recorded on a strip-chart running at 2 mm/minute. (c) and (d) Purified N68 was analyzed by gel filtration chromatography under the same conditions as the molecular mass standards. When applied to the column at 10 mg/ml (c), N68 eluted at 10.5 ml, corresponding to an M_R value of 250 kDa, but when loaded at 0.2 mg/ml (d), N68 eluted at 12 ml with an apparent M_R value of 115 kDa.

Table 1. Apparent M_R of N68 as a function of protein concentration

Species	Concentration (mg/ml)	Elution volume (ml)	Molecular mass (kDa)
SecA, Full Length	2	10.7	220
N68	10	10.5	250
N68	1	11.1	180
N68	0.5	11.6	140
N68	0.2	12.0	115
N68	0.1	12.3	98
N68	0.04	12.5	89

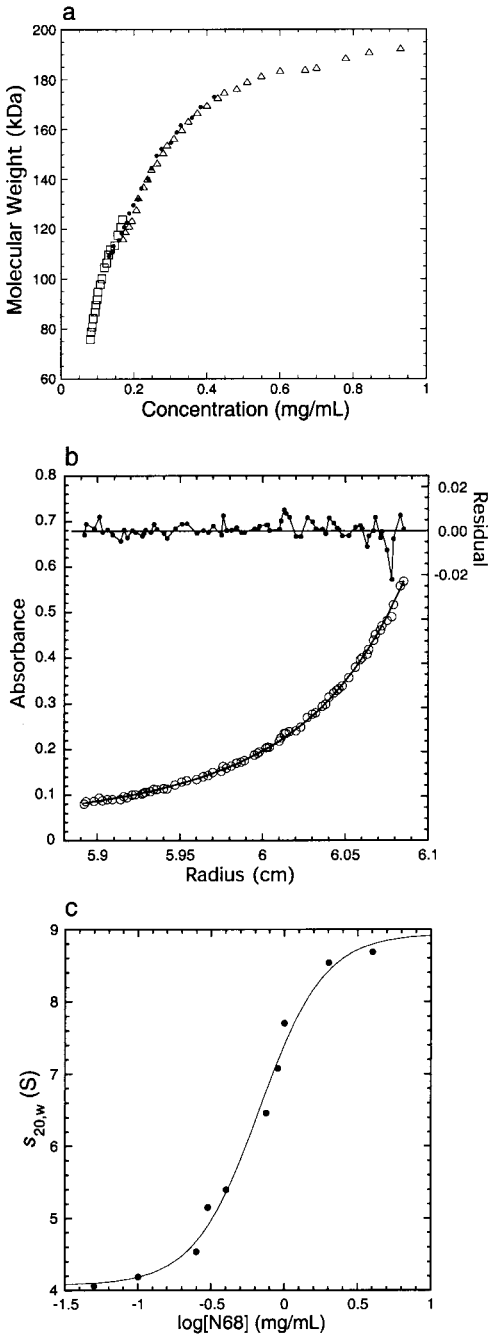

Figure 2. Self-association of N68. The molecular mass and hydrodynamic properties of N68 were assessed by sedimentation equilibrium ((a) and (b)) and sedimentation velocity (c). (a) N68 (2.8 mg/ml) was diluted to 0.7 mg/ml (triangles), 0.35 mg/ml (filled circles), or 0.14 mg/ml (squares), and brought to equilibrium at 10,000 rpm at which time the cells were scanned at 280 nm. Background absorbance was subtracted by meniscus depletion at the end of the experiment, yielding curves of protein absorbance *versus* radius. For each of these curves, a moving 40 point window used to calculate an ''instantaneous'' molecular mass at each point. For a reversibly self-associating system, the molecular masses will be dependent on equilibrium protein concentration only, and independent of starting concentration and rotor speed. (b) A solution of N68 (0.35 mg/ml) was placed in a six-sector cell, and brought to equilibrium at 7000, 8500, 10,000, and 13,000 rpm, with absorbance scans made at each rotor speed. The empty circles represent the absorbance at 280 nm measured for the inner-most sector of the cell at 10,000 rpm. An association constant describing a monomer-tetramer equilibrium for N68 was calculated by fitting the 12 curves (three data sets for each of four speeds) to an expression describing the equilibrium distribution of the two species. A dissociation constant of 63 μM^3 was obtained, and the theoretical curve for this model is illustrated by the continuous line. The calculated residuals are shown at the top of the graph. (c) Sedimentation velocity experiments were carried out with N68 at concentrations from 0.05 to 4 mg/ml, and for each experiment the average sedimentation coefficient was calculated from a $g^*(s)$ *versus* s plot.[55] The average sedimentation coefficients were plotted against the logarithm of protein concentration, and the data points were fitted to a biphasic sigmoidal growth model to obtain sedimentation coefficients for the limiting cases of very high and very low protein concentration.

dent. In summary, N68 undergoes a simple monomer-tetramer equilibrium with a K_D value of approximately 63 μM^3.

Hydrodynamic properties of N68: sedimentation velocity

Sedimentation velocity was used to examine the hydrodynamic properties of the individual N68 species. The conditions for these experiments were exactly the same as for the sedimentation equilibrium experiments, and it is therefore reasonable to assume that the solutions contain N68 monomers and tetramers. In all of the sedimentation velocity experiments, separate boundaries for the monomer and tetramer were not observed. Instead, the rapid equilibration between tetramer and monomer caused the protein to sediment with a single boundary moving at an averaged velocity. Therefore, to estimate the hydrodynamic properties of the N68 monomer and tetramer, sedimentation velocity experiments were conducted at different concentrations of N68 and a single sedimentation coefficient was calculated for each case. The sedimentation coefficient displayed a marked concentration dependence: N68 at 0.05 mg/ml sedimented with an of $s_{20,w}$ of 4.06 S, while at 4 mg/ml, $s_{20,w}$ was equal to 8.69 S (Figure 2(c)). Estimates for the sedimentation coefficients of pure monomer and tetramer were determined by fitting a plot of sedimentation coefficient *versus* protein concentration to a biphasic sigmoidal growth model (Figure 2(c)). The two molecular species were sufficient to model adequately the experimental data, and the sedimentation coefficients obtained from this analysis were $s_{20,w} = 4.07$ S for the monomer, $s_{20,w} = 8.94$ S for the tetramer (Table 2).

The sedimentation coefficients were used to calculate frictional ratios, f/f_{min}, for the monomer and tetramer, respectively (Table 2), which yield infor-

Table 2. Hydrodynamic properties of N68

Form	Mass (kDa)	$s_{20,w}$ (S)	f (s^{-1})	f/f_{min}	$D_{20,w}$ ($cm^2 \cdot s^{-1}$)
Monomer	68.4	4.07	7.34×10^{-8}	1.43	5.51×10^{-7}
Tetramer	274	8.94	1.34×10^{-7}	1.65	3.03×10^{-7}

mation about their shape. The monomer is similar in size to bovine serum albumin (66.5 kDa) and hemoglobin (68 kDa), which have frictional ratios of 1.33 and 1.28, respectively.[44] The modestly higher frictional ratio for the N68 monomer (1.43) indicates slightly greater asymmetry, but remains in the range for globular proteins. With a frictional ratio of 1.65, however, the N68 tetramer appears to be substantially less globular in shape. For reference, the full-length SecA dimer has a sedimentation coefficient, $s_{20,w}$, of 6.26 S and a frictional ratio of 1.95, consistent with previous SAXS work, suggesting that SecA was a highly extended molecule.[26]

Shape and conformation of N68: small-angle X-ray scattering

Small angle X-ray scattering (SAXS) yields information on the size and shape of molecules in solution. In particular, a Guinier plot[45] of SAXS data gives values for the radius of gyration, R_g (defined as the rms distance of all atoms from their common center of gravity), and the forward scattering, $I(0)$, which is proportional to the molecular mass of the scattering particle. Guinier curves for wild-type SecA and N68 are plotted in Figure 3(a); the linearity of the data in this region indicates a complete absence of high molecular mass aggregates for both proteins. Comparing the Guinier curve of N68 with that of full length SecA, both at a protein concentration of 6.7 mg/ml, it is clear that the intercept, $\ln[I(0)]$, of the N68 curve is larger while the slope, $-R_g^2$, is more negative, consistent with a higher molecular mass and larger R_g value for the N68 protein. N68 scattered with an apparent M_R of 246 kDa, an R_g value of 4.8 nm, and a maximal dimension of 13.5 nm, whereas similarly prepared full-length SecA scattered with a molecular mass of 200 kDa, an R_g value of 4.2 nm, and a maximal dimension of 13.0 nm. Note that the values for R_g and the maximal dimension of full-length SecA in this study are lower than those obtained previously (R_g was 4.47 nm and maximal dimension was 15 nm).[26] We attribute this difference to gel-filtration chromatography of the proteins prior to SAXS measurements in this study, which effectively removes strongly scattering (but low abundance) aggregates.

SAXS from N68 was measured at protein concentrations from 1.3 to 6.7 mg/ml (data not shown), and the forward scattering increased slightly with protein concentration. This was consistent with the dissociation constant calculated from analytical ultracentrifugation studies, which predicts that at 1.3 mg/ml approximately 80 % of the protein mass would be present as tetrameric N68, with the mass of tetramer increasing to 94 % of the total at 6.7 mg/ml. This 14 % change in the relative mass concentration of tetramer would be expected to produce a 10 % increase in the X-ray scattering, roughly what was observed. The forward scattering yields the average M_R value for all scattering species: for N68 at 6.7 mg/ml, the apparent M_R is 246 kDa, which is reasonably close to the expected M_R of 262 kDa for a mixture comprised of 94 % (by mass) tetramer (274 kDa) and 6 % monomer (68.5 kDa). The R_g value decreased slightly with increasing concentration, but this 1 % change is probably due to a small amount of interparticle interference, and is not experimentally significant.

These SAXS data were of sufficiently high quality to use a recently developed method[46] to calculate low resolution shapes for the scattering particles. The program *Saxs3D*[46] generates a shape for a given scattering curve by adding and removing spheres to lattice points in a hexagonally packed array. The process begins by placement of a single sphere, and continues by addition or removal of spheres, preferably at positions that neighbor the original sphere; each addition or removal is evaluated by scoring against a linear (as opposed to logarithmic) representation of the scattering curve. The overall effect is to gradually build up a structure consisting of densely packed spheres in such a way that the final shape is smooth and continuous, and conforms well to the lower-angle scattering data. The shapes obtained are not absolutely unique, and therefore to extract the ''essential'' or ''common'' shape information encoded in the scattering curve, the whole process is run a number of times and then the individual structures are superimposed using the program *xlattice*.[46] The lattice spacing can also be varied: larger lattice spacings correspond to larger spheres and fewer parameters, and therefore the fit to the experimental data is generally not as good as for smaller lattice spacings. On the other hand, if the lattice spacing is too small, there will be too many spheres (parameters) and the algorithm fails to converge. In this regard, it is important to note that the shape simply delineates the protein, a region of relatively high electron density, from the solvent, but does not provide any information on the ''higher-resolution'' features of the protein. Therefore, the high angle regions of the scattering curves, which are dependent on the finer structural features of the protein, cannot be reliably modelled using this type of *ab initio* process.

The *Saxs3D* algorithm requires data from $S = 0.0\ nm^{-1}$ to the highest angle measured,

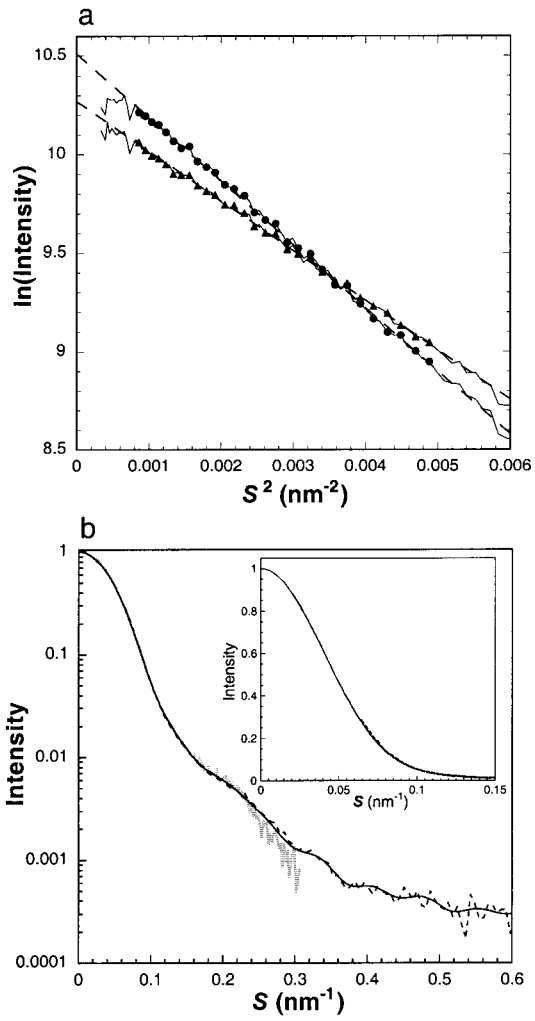

Figure 3. Small angle X-ray scattering from N68 and full-length SecA. (a) Guinier plots of SAXS from N68 at 6.7 mg/ml (circles) or full-length SecA at 7.6 mg/ml (triangles) illustrate differences in the radius of gyration and forward scattering for these molecules. The complete scattering data are represented by thin, continuous lines, while individual data points used for Guinier analysis are marked with circles or triangles. Linear least-squares fits to the Guinier equation[45] are indicated by the broken lines. (b) Data treatment for shape determination. A SAXS curve recorded from a 6.7 mg/ml solution of N68 with a 3 m sample-detector distance (thick grey curve) was combined with a second data set recorded from a 17 mg/ml solution of N68 using a 1.2 m sample-detector distance (broken curve). The data were scaled and merged using the program GNOM[47] and the combined data were used to calculate a regularized scattering curve extending from $S = 0$ nm^{-1} (black continuous curve). The inset shows the same data using a linear scale for the intensity and expanded to emphasize the region of momentum transfer, $0.0 < S < 0.15$ nm^{-1}, that is important for shape determination. The regularized data were used as input to the program *Saxs3D*.[46]

preferably at $S = 0.6$ nm^{-1} or greater. We merged two data sets to cover the large momentum transfer range required: the first data set ($0.02 < S < 0.3$ nm^{-1}) was recorded from a 6.7 mg/ml solution of N68, using a 3 m sample to detector distance, and the second data set ($0.06 < S < 0.8$ nm^{-1}) was recorded from a 17 mg/ml solution of N68 using a 1.2 m camera (Figure 3(b)). The two data sets were scaled and merged using the program GNOM;[47] after scaling and merging, a regularized scattering curve ($0.0 < S < 0.8$ nm^{-1}) was calculated and these data were used for shape determination by *Saxs3D*. Ten independent models were calculated for each of four lattice spacings: 2 nm, 1.6 nm, 1.4 nm, and 1.2 nm. Each set of ten models was superimposed using the program *xlattice*[46] and the final superposition was contrast filtered by removing atoms that had fewer than 40 neighbors. In this way, ''average'' structures were obtained that illustrate the conserved low-resolution features of the tetramer. We found that lattice spacings of 2.0 nm and 1.6 nm fit the experimental data to momentum transfer values of 0.1 nm^{-1} and 0.15 nm^{-1}, respectively (Figure 4(a) and (b)). In these cases, the shapes corresponded to rectangular ''boxes'' with dimensions of approximately 13.5 nm × 9.0 nm × 6.5 nm. Decreasing the lattice spacing to 1.4 nm resulted in a good fit to experimental data out to $S = 0.24$ nm^{-1}; the shapes obtained were similar to those found with larger spacings, but it became apparent in all of the 1.4 nm spaced structures that electron density in the middle part of the complex was relatively weak or non-existent, and the result was a pore in the contrast-filtered superposition (Figure 4(c)). A further decrease in the lattice spacing to 1.2 nm (Figure 4(d)) did not improve the fit of the models to the experimental data, except in the higher angle regions, and the models actually yielded poorer fits in the region $0.18 < S < 0.23$ nm^{-1}. Lattice spacings of 1.0 and 0.8 nm were also tested, but in these cases the program failed to converge on a solution. To summarize, the N68 tetramer is a flattened, extended particle with overall dimensions of 13.5 nm × 9.0 nm × 6.5 nm, and may contain a central pore.

It has been shown that N68 becomes resistant to proteolysis when it binds ADP but not AMP-PNP, indicating that ADP binding causes a conformational change in N68.[32,39] SAXS provides a direct measure of conformational change, and we therefore added either ADP or AMP-PNP at saturating concentrations (2 mM, a 20-fold molar ratio over protein) to our SAXS solutions. Consistent with the results for full-length SecA,[26] there was no change in either the R_g, the maximal dimension (d_{max}), or the apparent molecular mass of N68 after addition of nucleotides. Changes in these parameters, which are reflected in the low angle parts of the scattering curves, would require large-scale domain movements. At higher angles, scattering becomes sensitive to smaller changes in protein conformation. We used Kratky plots, $S^2I(S)$ *versus* S, to compare unliganded N68 with nucleotide-

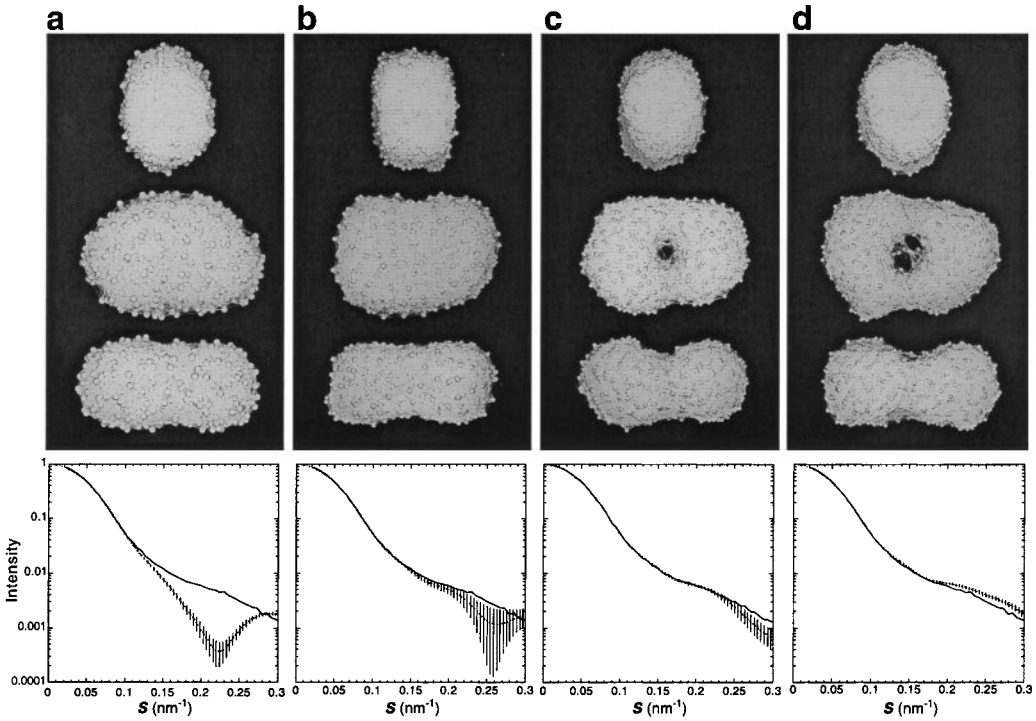

Figure 4. The shape of the N68 tetramer. The programs *Saxs3D* and *xlattice*[46] were used to calculate shapes from regularized SAXS data ($0 < S < 0.8$ nm^{-1}) using lattice spacings of (a) 2.0 nm, (b) 1.6 nm, (c) 1.4 nm or (d) 1.2 nm. In each case, ten structures were calculated by successive runs of *Saxs3D* and then superimposed using *xlattice*;[46] the superposition was contrast filtered to illustrate common features of the shapes. The graphs at the bottom of each panel show the experimental data (continuous curve) with a curve (broken with error bars) that represents the average calculated scattering from each of the ten superimposed structures. The error bars are the standard deviations of the ten calculated curves at each S value.

bound forms of the enzyme; these plots emphasize mid-range momentum transfer values ($0.05 < S < 0.15$ nm^{-1}). Close inspection of the entire scattering curves indicates that AMP-PNP has no observable effect on the conformation of the protein (Figure 5(a)). Data in the higher angle regions, $0.15 < S < 0.3$ nm^{-1}, is heavily influenced by the buffer subtraction, and therefore differences in the curves cannot be reliably attributed to changes in protein conformation. In the case of N68 with 2 mM ADP, there was a small change in the region $0.08 < S < 0.11$ nm^{-1} when compared to unliganded N68 (Figure 5(b), inset). Because the curves for unliganded and ADP-bound N68 coincide both before and after this region, the change is not artifactual and must represent a small conformational shift in the N68 tetramer upon ADP binding.

Discussion

When separated from the C-terminal 34 kDa domain, the 68 kDa ATPase domain of SecA can form a tetramer. We have determined a K_D value of 63 μM[3] for the monomer-tetramer equilibrium, allowing calculation of the concentration of tetramer as a function of total protein concentration (Figure 6). The N68 tetramer was not observed in previous studies because the concentrations used for cross-linking and gel-filtration were in the range from 0.1 to 0.3 mg/ml, just below the regime where the tetramer dominates.[38,39]

Nucleotide binding and hydrolysis are critical for preprotein translocation[15] and drive conformational changes in SecA that affect its interaction with SecYEG;[13,17] we were therefore interested to see how binding of nucleotide affected the structure of N68. Previous SAXS studies on full-length SecA indicated that the protein in solution does not undergo a large-scale conformational change as a result of binding ADP, ATP, or AMP-PNP.[26] On the other hand, evidence for conformational changes in solution comes from the fact that ADP-bound SecA is partially protected from protease,[29,39] and from changes in tryptophan fluorescence and stability upon nucleotide binding[28] and CD spectroscopy.[32] One can conclude from these results that, in solution, SecA undergoes small-scale nucleotide-dependent conformational changes. The situation appears to be similar for the isolated ATPase domain: this domain is stabilized against tryptic digestion by ADP but not AMP-PNP, and therefore ADP must change the conformation of N68 to some degree.[39] The SAXS studies we have carried out with N68 show that there is no detectable change wrought by AMP-PNP bind-

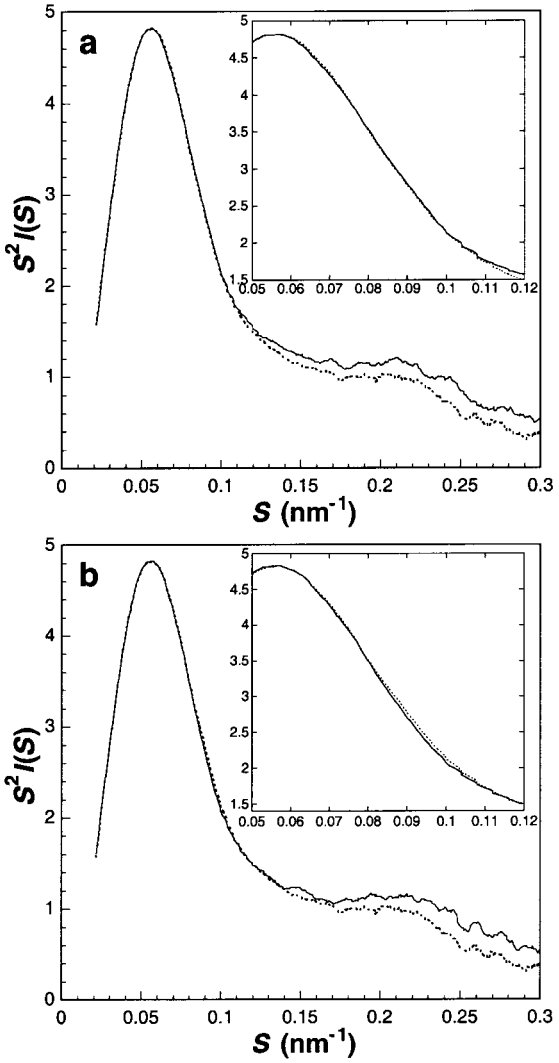

Figure 5. Effect of nucleotides on N68 conformation. Kratky plots, $S^2I(S)$ *versus* S, of N68 (6.5 mg/ml) in the absence of nucleotides (dotted curves in both (a) and (b)) and in the presence of (a) 2 mM AMP-PNP or, (b) 2 mM ADP. Insets have been expanded to emphasize momentum transfer values in the range $0.05 < S < 0.11$ nm^{-1}. Scattering curves were recorded with a 3 m camera setting using a Quadrant segment-shaped detector.

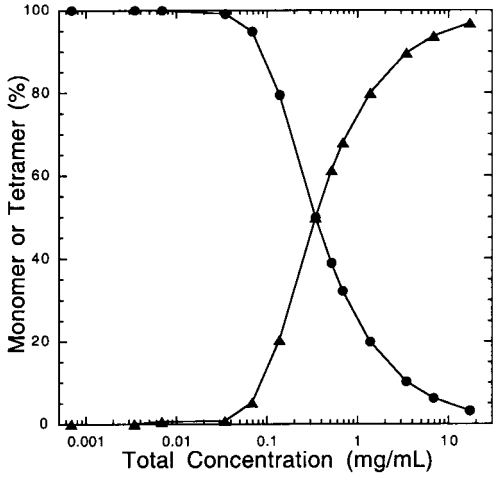

Figure 6. Total protein concentration and percentage of tetramer. The equation relating the dissociation of tetramer, $K_D = [\text{monomer}]^4/[\text{tetramer}]$, was combined with a mass balance equation and solved numerically to yield the concentrations of monomer (circles) and tetramer (triangles) over a range of total protein concentration.

ing, and a barely detectable conformational change upon ADP binding. Thus, in solution, the conformational changes caused by ADP binding are relatively minor and do not involve large domain movements or rearrangements.

The behaviour of N68 in sedimentation velocity experiments indicates that the monomer is close to globular in shape, but the tetramer, with its high frictional ratio, is more ellipsoidal. To obtain more detailed structural information, a molecular envelope for the N68 tetramer was calculated using SAXS data. The shape that emerged from this SAXS analysis is a 13.5 nm × 9.0 nm × 6.5 nm "box", and when finer lattice spacings were used for the structure determination, a pore appeared roughly in the middle of the structure. This irregular shape for the N68 tetramer is consistent with its high frictional ratio determined by sedimentation velocity analysis. A final issue is the symmetry of the tetramer, which could be either *D*2 or *C*4 (Figure 7(a)). The shapes obtained *ab initio* from the SAXS data appear to conform to *D*2 symmetry.

The existence of the N68 tetramer changes our view of the domain structure of SecA, in which it was previously thought that the C-terminal 34 kDa domain was solely responsible for protomer interactions. It is clear that the C-terminal domain plays a key role in dimerization because its removal results in the appearance of monomeric N68, and the isolated C-terminal domain itself forms dimers.[38,39] However, the presence of the N68 tetramer demonstrates that the N-terminal ATPase domain has the ability to mediate protomer-protomer interactions: these same interactions may occur within a SecA dimer. Given that the nucleotide, preprotein, and SecY binding sites reside on N68,[34,35,37] direct interactions between the N-terminal ATPase domains of the SecA molecule may be important in the regulation and catalysis of translocation.

The physiological role of the N68 tetramer remains an open question, and the possibility that the tetramer is an *in vitro* artifact resulting from removal of the C-terminal domain cannot be ruled out. Clearly, removal of the C-terminal domain exposes a surface on N68, and/or causes a conformational change, that mediates oligomerization to a tetramer. Higher oligomers were not observed even at very high protein concentrations; furthermore, we have produced large

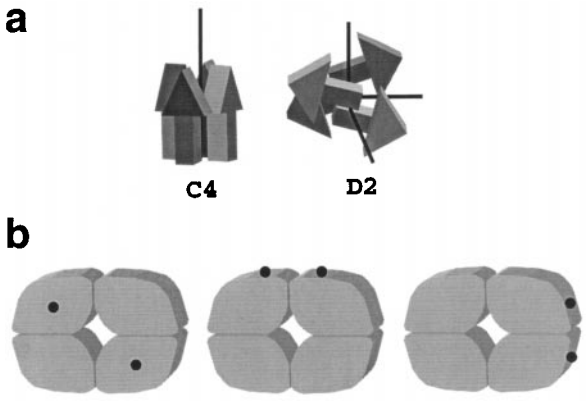

Figure 7. Structural models for the N68 tetramer. (a) A tetramer composed of four identical protomers can be assembled using two possible symmetries: *C*4 (on the left), with a single 4-fold axis relating the protomers; or *D*2 (on the right), with three mutually perpendicular 2-fold axes. (b) Using *D*2 symmetry and a slightly extended protomer, models for the N68 tetramer can be constructed. In each case, possible SecYEG binding sites[37] are indicated by black dots. Assuming one SecYEG binding site per protomer, there will be four binding sites per tetramer related by *D*2 symmetry (only two binding sites are visible in each of the three cases).

(0.3 mm × 0.3 mm × 0.3 mm), well-formed crystals of N68 that diffract up to 10 Å resolution using a laboratory X-ray source. From these results, we conclude that the interactions between N68 monomers are specific, such that a homogeneous population of tetrameric N68 is produced. Our observations do not constitute evidence that a related structure occurs *in vivo*, but they are at least consistent with a potential physiological role for the tetramer.

One intriguing possibility is that the N68 tetramer may represent part of a higher-order structure that is assembled when SecA interacts with preprotein, ATP, and SecYEG during active translocation; that is, conformational changes at the membrane may uncover the same surfaces that are exposed when the C-terminal domain is removed. When SecA interacts with SecY[48,49] through its N-terminal[37] and/or C-terminal domain,[50] there is an increase in ATP-driven proteolytic stability[13] that is fundamentally different from what is observed when SecA binds ATP in solution.[39] Interestingly, there is also evidence that interaction between SecA and SecYEG changes the oligomeric structure of SecYEG. Two recent papers have shown that detergent-solubilized SecYEG exists predominantly as monomers and dimers,[22,23] but that interaction with SecA results in the formation of a tetramer.[23]

To explore a possible role for the tetramer, a rough model can be constructed using the results from the present study. Given *D*2 symmetry, the N68 tetramer can be divided into four slightly extended pieces representing the N68 protomers. Each N68 protomer contains a SecYEG binding site:[37] these binding sites can be located anywhere on the monomer, but the *D*2 symmetry dictates their relative position on the tetramer; that is, the SecYEG binding sites on the tetramer must be related by the three 2-fold axes (Figure 7(b)). We have presented three possible alternatives for the location of the SecYEG binding sites to illustrate how they would be related by the *D*2 symmetry of the particle. Note that the SecYEG binding sites could also be located in the interfaces between protomers, in which case the tetramer would not be expected to bind to SecYEG.

There are still many unanswered questions regarding the structure and oligomeric composition of the translocon, and the ability of the N-terminal ATPase domain of SecA to mediate tetramer formation should be taken into consideration as models are developed. Understanding the function of the N68 tetramer in protein translocation will require further structural studies of the SecA-SecYEG complex.

Materials and Methods

Expression and purification of N68

E. coli BL21-19(DE3), transformed with vector pIMBB7,[32] were used to express hexa-histidine tagged *E. coli* N68 in a 36 l fermentor. Cells were grown at 30 °C in regular LB broth with 270 μM ampicillin to an A_{600} of 0.4-0.5, and then induced by addition of 420 μM IPTG. Cells were harvested three hours later using a tangential flow concentrator (Amicon), resuspended in 50 mM Tris-HCl (pH 8.0), and broken open using a French press. Several additions of PMSF (1 mM final concentration) were added to inhibit proteolysis. The lysate was cleared by centrifugation at 100,000 ***g*** for one hour. A crude extract containing N68 was produced by taking a 20-50 % ammonium sulfate cut at 0 °C. The ammonium sulfate pellet was dissolved in 50 mM sodium phosphate (pH 7.5), and the crude extract was flash frozen and stored at −80 °C.

The crude extract was thawed and supplemented with potassium chloride to a final concentration of 1 M and imidazole to a concentration of 40 mM. The solution was then applied to a 1.6 cm × 12 cm column of chelating Sepharose Fast-Flow (Pharmacia), that had been loaded with Ni^{2+} and equilibrated with 50 mM sodium phosphate, 1 M KCl, 40 mM imidazole (pH 7.5). After extensive washing, bound N68 was eluted with 50 mM sodium phosphate, 1 M KCl, 250 mM imidazole (pH 7.5). The protein was then dialyzed against 50 mM Tris-HCl (pH 7.8). Additional purification of N68 was effected using anion-exchange chromatography on a 2.6 cm × 18 cm column of Q-Sepharose HP (Pharmacia) with a running buffer of 50 mM Tris-HCl buffer (pH 7.8) and a 500 ml linear salt gradient from 0 to 500 mM NaCl. N68 emerged from the column at approximately 300 to 350 mM NaCl.

Protein concentrations were assayed using the method of Bradford.[51] Alternatively, an extinction coefficient for N68 of 48600 $M^{-1} \cdot cm^{-1}$ (280 nm) was determined as follows: an aliquot of dialyzed N68 was diluted into a guanidine-HCl solution so that the final mixture consisted of 6 M guanidine-HCl, 20 mM sodium phosphate (pH 6.5). Under these conditions, and based on the content of aro-

matic residues inferred from the DNA sequence, denatured N68 should have an extinction coefficient at 280 nm of 37550 $M^{-1} \cdot cm^{-1}$,[52] allowing us to determine the protein concentration in the original N68 solution. The absorbance (280 nm) of the N68 solution under non-denaturing conditions was measured and related to the protein concentration to obtain the extinction coefficient. For non-reducing SDS-PAGE, samples were heated in buffer containing 15 mM *N*-ethylmaleimide to block any free sulfhydryl groups and prevent disulfide exchange.

Molecular weight determination by gel filtration chromatography

Analytical gel filtration chromatography was carried out at 20 °C using a 1.0 cm × 30 cm Superdex 200 HR column coupled to an FPLC (Pharmacia). The running buffer was composed of 50 mM Tris-HCl, 100 mM KCl, 5 mM $MgCl_2$, 1 mM EDTA, and 5 mM β-mercaptoethanol (pH 8.0). Sample volumes of 100 µl were injected onto the column and eluted at a flow rate of 0.5 ml/minute. The optical density of the eluent was measured at 280 nm and recorded on a strip-chart running at 2 mm/minute. The column was calibrated with blue dextran (void volume), acetone (included volume), ferritin (440 kDa), pyruvate kinase (232 kDa), yeast alcohol dehydrogenase (150 kDa), horse liver alcohol dehydrogenase (80 kDa), ovalbumin (45 kDa), carbonic anhydrase (29 kDa) and ribonuclease A (13.7 kDa).

Analytical ultracentrifugation

Prior to sedimentation analysis, samples were supplemented with 50 mM DTT to ensure full reduction of the single cysteine present in N68. The reduced solution was then dialyzed exhaustively against 50 mM Tris, 100 mM KCl, 5 mM $MgCl_2$, 1 mM EDTA, 2 mM DTT (pH 8); dialysis buffer was saved and used in the reference sector for all runs. A partial specific volume for N68 of 0.734 ml/g at 20 °C was calculated from the amino acid composition of the protein.[53] The density of the solvent at 20 °C was calculated to be 1.0049 g/ml.[54] Analytical ultracentrifugation was carried out in a Beckman XL-A centrifuge with a four-hole An-60Ti rotor. Whenever possible, absorbance measurements were made at 280 nm; alternatively, for dilute or concentrated samples, shorter (230 or 235 nm) or longer (295 nm or above) wavelengths were used to bring the absorbance readings into the range from 0.1 to 1.0. Unless otherwise specified, all data analyses were carried out using the Beckman Origin 4.0 software. For sedimentation equilibrium runs, cells incorporating 6-sector Epon charcoal centerpieces were used. Absorbance measurements were taken in 0.002 cm radial steps and averaged over ten observations. Equilibrium was attained when absorbance scans taken over five hours apart were identical. The baseline absorbance was measured after increasing the rotor speed to 40,000 rpm to deplete the sectors of protein.

Sedimentation velocity analyses were carried out at 20 °C in cells containing double-sector Epon charcoal centerpieces. Velocity runs for N68 were conducted at 30,000-40,000 rpm depending on whether monomer or tetramer was expected to predominate. Absorbance measurements were taken in 0.005 cm radial steps and averaged over five observations. The cells were scanned every ten minutes for a total of 300 minutes. Sedimentation coefficients were calculated using the time derivative (dc/dt) analysis of Stafford[55] and the peak of the $g^*(s)$ *versus* s plot was fitted using a Gaussian distribution. The $s_{20,w}$ values for pure monomer and tetramer were estimated by assuming that the apparent sedimentation coefficient was equal to the weight average sedimentation coefficient (equation (1)), which can be rearranged to yield equation (2):

$$\bar{s}_{20,w} = \frac{[\text{monomer}] \times s_{20,w,\text{monomer}} + [\text{tetramer}] \times s_{20,w,\text{tetramer}}}{[\text{monomer}] + [\text{tetramer}]} \quad (1)$$

$$\bar{s}_{20,w} = s_{20,w,\text{monomer}} + \frac{[\text{tetramer}]}{[\text{monomer}] + [\text{tetramer}]} \times (s_{20,w,\text{tetramer}} - s_{20,w,\text{monomer}}) \quad (2)$$

where [monomer] and [tetramer] are mass concentrations, and $s_{20,w,\text{monomer}}$ and $s_{20,w,\text{tetramer}}$ are the sedimentation coefficients of the pure monomer and tetramer, respectively. The form of equation (2) resembles a biphasic sigmoidal growth model in which one species (monomer) is converted into a second species (tetramer) in response to changes in a given factor (in this case, total protein concentration):

$$\bar{s}_{20,w} = s_{20,w,\text{monomer}} + \frac{1}{1 + 10^{(\log EC50 - \log[\text{N68}]) \times slope}} \times (s_{20,w,\text{tetramer}} - s_{20,w,\text{monomer}}) \quad (3)$$

Where [N68] is the total protein concentration. The sedimentation coefficients were fit to equation (3), varying the $s_{20,w}$ values for pure monomer and tetramer, as well as the *EC50* value (midpoint of curve) and *slope*. The *EC*50 value and *slope* do not have any physical meaning in the context of our monomer-tetramer association, but provide an adequate description of the transition from monomer to tetramer as a function of total protein concentration. Frictional coefficients (f), frictional ratios ($f/f_{\min}$), and diffusion coefficients ($D_{20,w}$) were calculated from $s_{20,w}$ and M_R by standard methods.

SAXS

Gel filtration chromatography was used to eliminate any large aggregates in the protein preparations and ensure the highest quality SAXS data. Several days prior to SAXS experiments, proteins were purified by preparative gel filtration chromatography using a 2.6 cm × 60 cm column of Superdex 200 HR Prep Grade chromatography resin (Pharmacia), with a running buffer composed of 50 mM Tris-HCl, 100 mM KCl, 5 mM $MgCl_2$, 1 mM EDTA, and 5 mM β-mercaptoethanol (pH 8). After this treatment, the protein preparations were concentrated, dialyzed, and maintained on ice. The dialysis buffers were reserved for background measurements (see below).

All measurements were made at the European Molecular Biology Laboratory Outstation at the Deutsches Elektronen-Synchrotron (Hamburg, Germany), beamline X33,[56] at 15 °C using radiation with a wavelength of 0.15 nm. Measurements were made using either a position-sensitive linear detector or a Quadrant segment-shaped multiwire detector.[57,58] Sample-detector distances of 1.2 m (high angle) and 3 m (low angle) were used to cover the range of momentum transfer ($S = 2\sin\theta/\lambda$, where 2θ is the scattering angle) from 0.02 to 0.8 nm^{-1}.

Fifteen successive one minute exposures were recorded for each sample; there was no evidence of protein degradation over this time interval. Recording of each protein sample was preceded and followed by recording from the buffer alone: these buffer measurements were compared and provided a check on beam properties, cell contamination, and so on. Averaging of frames, corrections for detector response and beam intensity, and buffer subtraction, were done using the programs SAPOKO (D. I. Svergun & M. H. J. Koch, unpublished results) and OTOKO.[59]

The radius of gyration (R_g) is defined as the root-mean-square distance of all atoms from their common center of mass. The forward scattering, $I(0)$, is the X-ray scattering that is parallel to the incident beam and must be determined by extrapolation of the experimental data. Both the R_g and $I(0)$ values were determined from the distance distribution function, $P(r)$, after regularization and transformation by GNOM.[47] The forward scattering is proportional to the product of the molecular mass and concentration of the scattering particle. Solutions of BSA at 7.0 mg/ml were used to calibrate the system.

Acknowledgments

The expert assistance of Michel Koch at beamline X33 is gratefully acknowledged. We thank L. Karamanou for useful discussions. The analytical ultracentrifugation studies were carried out in the Biomolecular Interaction and Conformation Facility at the University of Western Ontario. Supported by European Union grants Biotech2-BIO4-CT97-2244, QLK3-CT-2000-00082, QLRT-2000-00122 and RTN1-1999-00149 (to A.E.), Canadian Institutes for Health research grant MT-10237 (to S.D.D.), and Canadian Institutes for Health research grant MT-15624 (to B.H.S.).

References

1. Driessen, A. J., Manting, E. H. & van der Does, C. (2001). The structural basis of protein targeting and translocation in bacteria. *Nature Struct. Biol.* **8**, 492-498.
2. Economou, A. (2000). Bacterial protein translocase: a unique molecular machine with an army of substrates. *FEBS Letters,* **476**, 18-21.
3. Müller, M., Koch, H. G., Beck, K. & Schafer, U. (2000). Protein traffic in bacteria: multiple routes from the ribosome to and across the membrane. *Prog. Nucl. Acid Res. Mol. Biol.* **66**, 107-157.
4. Brundage, L., Hendrick, J. P., Schiebel, E., Driessen, A. J. & Wickner, W. (1990). The purified *E. coli* integral membrane protein SecY/E is sufficient for reconstitution of SecA-dependent precursor protein translocation. *Cell,* **62**, 649-657.
5. Brundage, L., Fimmel, C. J., Mizushima, S. & Wickner, W. (1992). SecY, SecE, and band 1 form the membrane-embedded domain of *Escherichia coli* preprotein translocase. *J. Biol. Chem.* **267**, 4166-4170.
6. Douville, K., Price, A., Eichler, J., Economou, A. & Wickner, W. (1995). SecYEG and SecA are the stoichiometric components of preprotein translocase. *J. Biol. Chem.* **270**, 20106-20111.
7. Hartmann, E., Sommer, T., Prehn, S., Gorlich, D., Jentsch, S. & Rapoport, T. A. (1994). Evolutionary conservation of components of the protein translocation complex. *Nature,* **367**, 654-657.
8. Johnson, A. E. & van Waes, M. A. (1999). The translocon: a dynamic gateway at the ER membrane. *Annu. Rev. Cell Dev. Biol.* **15**, 799-842.
9. Simon, S. M. & Blobel, G. (1992). Signal peptides open protein-conducting channels in *E. coli*. *Cell,* **69**, 677-684.
10. Joly, J. C. & Wickner, W. (1993). The SecA and SecY subunits of translocase are the nearest neighbors of a translocating preprotein, shielding it from phospholipids. *EMBO J.* **12**, 255-263.
11. Lill, R., Cunningham, K., Brundage, L., Ito, K., Oliver, D. & Wickner, W. (1989). The SecA protein hydrolyzes ATP and is an essential component of the protein translocation ATPase of *E. coli*. *EMBO J.* **8**, 961-966.
12. Lill, R., Dowhan, W. & Wickner, W. (1990). The ATPase activity of SecA is regulated by acidic phospholipids, SecY, and the leader and mature domains of precursor proteins. *Cell,* **60**, 271-280.
13. Economou, A. & Wickner, W. (1994). SecA promotes preprotein translocation by undergoing ATP-driven cycles of membrane insertion and deinsertion. *Cell,* **78**, 835-843.
14. Eichler, J. & Wickner, W. (1997). Both an N-terminal 65 kDa domain and a C-terminal 30 kDa domain of SecA cycle into the membrane at SecYEG during translocation. *Proc. Natl Acad. Sci. USA,* **94**, 5574-5581.
15. Schiebel, E., Driessen, A. J. M., Hartl, F.-U. & Wickner, W. (1991). $\Delta\mu_H^+$ and ATP function at different steps of the catalytic cycle of preprotein translocase. *Cell,* **64**, 927-939.
16. van der Wolk, J. P., de Wit, J. G. & Driessen, A. J. (1997). The catalytic cycle of the *Escherichia coli* SecA ATPase comprises two distinct preprotein translocation events. *EMBO J.* **16**, 7297-7304.
17. Economou, A., Pogliano, J. A., Beckwith, J., Oliver, D. B. & Wickner, W. (1995). SecA membrane cycling at SecYEG is driven by distinct ATP binding and hydrolysis events and is regulated by SecD and SecF. *Cell,* **83**, 1171-1181.
18. van der Does, C., Manting, E. H., Kaufmann, A., Lutz, M. & Driessen, A. J. (1998). Interaction between SecA and SecYEG in micellar solution and formation of the membrane-inserted state. *Biochemistry,* **37**, 201-210.
19. Kim, Y. J., Rajapandi, T. & Oliver, D. (1994). SecA protein is exposed to the periplasmic surface of the *E. coli* inner membrane in its active state. *Cell,* **78**, 845-853.
20. Ramamurthy, V. & Oliver, D. (1997). Topology of the integral membrane form of *Escherichia coli* SecA protein reveals multiple periplasmically exposed regions and modulation by ATP binding. *J. Biol. Chem.* **272**, 23239.
21. Eichler, J. & Wickner, W. (1998). The SecA subunit of *Escherichia coli* preprotein translocase is exposed to the periplasm. *J. Bacteriol.* **180**, 5776-5779.
22. Collinson, I., Breyton, C., Duong, F., Tziatzios, C., Schubert, D., Or, E. *et al*. (2001). Projection structure and oligomeric properties of a bacterial core protein translocase. *EMBO J.* **20**, 2462-2471.
23. Manting, E. H., van Der Does, C., Remigy, H., Engel, A. & Driessen, A. J. (2000). SecYEG assembles into a tetramer to form the active protein translocation channel. *EMBO J.* **19**, 852-861.

24. Yahr, T. L. & Wickner, W. T. (2000). Evaluating the oligomeric state of SecYEG in preprotein translocase. *EMBO J.* **19**, 4393-4401.
25. Akita, M., Shinaki, A., Matsuyama, S. & Mizushima, S. (1991). SecA, an essential component of the secretory machinery of *Escherichia coli*, exists as homodimer. *Biochem. Biophys. Res. Commun.* **174**, 211-216.
26. Shilton, B., Svergun, D. I., Volkov, V. V., Koch, M. H., Cusack, S. & Economou, A. (1998). *Escherichia coli* SecA shape and dimensions. *FEBS Letters,* **436**, 277-282.
27. Driessen, A. J. M. (1993). SecA, the peripheral subunit of the *Escherichia coli* precursor protein translocase, is functional as a dimer. *Biochemistry,* **32**, 13190-13197.
28. den Blaauwen, T., Fekkes, P., de Wit, J. G., Kuiper, W. & Driessen, A. J. M. (1996). Domain interactions of the peripheral preprotein translocase subunit SecA. *Biochemistry,* **35**, 11994-12004.
29. Shinkai, A., Mei, L. H., Tokuda, H. & Mizushima, S. (1991). The conformation of SecA, as revealed by its protease sensitivity, is altered upon interaction with ATP, presecretory proteins, everted membrane vesicles, and phospholipids. *J. Biol. Chem.* **266**, 5827-5833.
30. Price, A., Economou, A., Duong, F. & Wickner, W. (1996). Separable ATPase and membrane insertion domains of the SecA subunit of preprotein translocase. *J. Biol. Chem.* **271**, 31580-31584.
31. Koonin, E. V. & Gorbalenya, A. E. (1992). The superfamily of UvrA-related ATPases includes three more subunits of putative ATP-dependent nucleases. *Protein Seq. Data Anal.* **5**, 43-45.
32. Sianidis, G., Karamanou, S., Vrontou, E., Boulias, K., Repanas, K., Kyrpides, N. *et al*. (2001). Cross-talk between catalytic and regulatory elements in a DEAD motor domain is essential for SecA function. *EMBO J.* **20**, 961-970.
33. Walker, J. E., Saraste, M., Runswick, M. J. & Gay, N. J. (1982). Distantly related sequences in the α- and β-subunits of ATP synthase, myosin, kinases and other ATP-requiring enzymes and a common nucleotide binding fold. *EMBO J.* **1**, 945-951.
34. Mitchell, C. & Oliver, D. (1993). Two distinct ATP-binding domains are needed to promote protein export by *Escherichia coli* SecA ATPase. *Mol. Microbiol.* **10**, 483-497.
35. Kimura, E., Akita, M., Matsuyama, S. & Mizushima, S. (1991). Determination of a region in SecA that interacts with presecretory proteins in *Escherichia coli*. *J. Biol. Chem.* **266**, 6600-6606.
36. Triplett, T. L., Sgrignoli, A. R., Gao, F. B., Yang, Y. B., Tai, P. C. & Gierasch, L. M. (2001). Functional signal peptides bind a soluble N-terminal fragment of SecA and inhibit its ATPase activity. *J. Biol. Chem.* **276**, 19648-19655.
37. Dapic, V. & Oliver, D. (2000). Distinct membrane binding properties of N- and C-terminal domains of *Escherichia coli* SecA ATPase. *J. Biol. Chem.* **275**, 25000-25007.
38. Hirano, M., Matsuyama, S. & Tokuda, H. (1996). The carboxyl-terminal region is essential for Sec-A dimerization. *Biochem. Biophys. Res. Commun.* **229**, 90-95.
39. Karamanou, S., Vrontou, E., Sianidis, G., Baud, C., Roos, T., Kuhn, A. *et al*. (1999). A molecular switch in SecA protein couples ATP hydrolysis to protein translocation. *Mol. Microbiol.* **34**, 1133-1145.
40. Fekkes, P., van der Does, C. & Driessen, A. J. (1997). The molecular chaperone SecB is released from the carboxy-terminus of SecA during initiation of precursor protein translocation. *EMBO J.* **16**, 6105-6113.
41. Topping, T. B., Woodbury, R. L., Diamond, D. L., Hardy, S. J. & Randall, L. L. (2000). Direct demonstration that homotetrameric chaperone SecB undergoes a dynamic dimer-tetramer equilibrium. *J. Biol. Chem.* **7**, 7437-7441.
42. Xu, Z., Knafels, J. D. & Yoshino, K. (2000). Crystal structure of the bacterial protein export chaperone SecB. *Nature Struct. Biol.* **7**, 1172-1177.
43. McRorie, D. K. & Voelker, P. J. (1993). *Self-Associating Systems in the Analytical Ultracentrifuge*, Beckman Instruments, Fullerton, California.
44. Kuntz, I. D., Jr & Kauzmann, W. (1974). Hydration of proteins and polypeptides. *Adv. Protein Chem.* **28**, 239-345.
45. Guinier, A. & Fournet, G. (1955). *Small Angle Scattering of X-rays*, Wiley, New York.
46. Walther, D., Cohen, F. E. & Doniach, S. (2000). Reconstruction of low-resolution three-dimensional density maps from one-dimensional small-angle X-ray solution scattering data for biomolecules. *J. Appl. Crystallog.* **33**, 350-363.
47. Semenyuk, A. V. & Svergun, D. I. (1991). GNOM - a program package for small-angle scattering data processing. *J. Appl. Crystallog.* **24**, 537-540.
48. Hartl, F.-U., Lecker, S., Schiebel, E., Hendrick, J. P. & Wickner, W. (1990). The binding cascade of SecB to SecA to SecY/E mediates preprotein targeting to the *E. coli* plasma membrane. *Cell,* **63**, 269-279.
49. Manting, E. H., van der Does, C. & Driessen, A. J. (1997). *In vivo* cross-linking of the SecA and SecY subunits of the *Escherichia coli* preprotein translocase. *J. Bacteriol.* **179**, 5699-5704.
50. Snyders, S., Ramamurthy, V. & Oliver, D. (1997). Identification of a region of interaction between *Escherichia coli* SecA and SecY proteins. *J. Biol. Chem.* **272**, 11302-11306.
51. Bradford, M. M. (1976). A rapid and sensitive method for the quantitation of microgram quantities of protein utilizing the principle of protein-dye binding. *Anal. Biochem.* **72**, 248-254.
52. Gill, S. C. & von Hippel, P. H. (1989). Calculation of protein extinction coefficients from amino acid sequence data. *Anal. Biochem.* **182**, 319-326.
53. Cohn, E. J. & Edsall, J. T. (1943). In *Proteins, Amino Acids, and Peptides*, pp. 157-161, Reinhold, New York.
54. Laue, T. M., Shah, B. D., Ridgeway, T. M. & Pelletier, S. L. (1992). Computer-aided interpretation of analytical sedimentation data for proteins. In *Analytical Ultracentrifugation in Biochemistry and Polymer Science* (Harding, S. E., Rowe, A. J. & Horton, J. C., eds), pp. 90-125, Royal Society of Chemistry, Cambridge, UK.
55. Stafford, W. F., III (1992). Boundary analysis in sedimentation transport experiments: a procedure for obtaining sedimentation coefficient distributions using the time derivative of the concentration profile. *Anal. Biochem.* **203**, 295-301.
56. Koch, M. H. J. & Bordas, J. (1983). X-ray diffraction and scattering on disordered systems using synchrotron radiation. *Nucl. Instrum. Methods,* **208**, 461-469.
57. Gabriel, A. & Dauvergne, F. (1982). The localisation method used at EMBL. *Nucl. Instrum. Methods,* **201**, 223-224.

58. Boulin, C. J., Kempf, R., Gabriel, A. & Koch, M. H. J. (1988). Data acquisition systems for linear and area X-ray detectors using delay line readout. *Nucl. Instrum. Methods,* **A269**, 312-320.

59. Boulin, C., Kempf, R., Koch, M. H. J. & McLaughlin, S. (1986). Data appraisal, evaluations and display for synchrotron radiation experiments: hardware and software. *Nucl. Instrum. Methods,* **A249**, 399-407.

Edited by I. B. Holland

(Received 2 July 2001; received in revised form 16 November 2001; accepted 17 November 2001)